



Comparison of microalgal hydrochar and pyrochar: production, physicochemical properties, and environmental application

Chaerin Park¹ · Eun Jung Kim¹

Received: 13 August 2023 / Accepted: 28 November 2023 / Published online: 8 December 2023
© The Author(s), under exclusive licence to Springer-Verlag GmbH Germany, part of Springer Nature 2023

Abstract

Microalgal biomass has been considered the third-generation biofuel production feedstock, but microalgae-derived biochar still needs to be thoroughly understood. This study aims to evaluate the production and physicochemical properties of microalgae-derived hydrochar produced by hydrothermal carbonization (HTC) process by comparison with pyrochar produced by dry thermal carbonization (DTC) process for environmental applications. Microalgal biochar was produced with commercially available *Chlorella vulgaris* microalgae using HTC and DTC processes under various temperature conditions. Pyrochar presented higher pH, ash contents, porosity, and surface area than hydrochar. Hydrochar gave more oxygen-containing functional groups on the surface and higher lead adsorption than pyrochar, making the microalgal hydrochar applicable in soil amendment and various environmental remediations. HTC could be an economically feasible thermochemical process for microalgal biochar production. It can produce hydrochar with high production yield from wet microalgae at low temperatures without a drying process.

Keywords Hydrochar · Pyrochar · Microalgae · Hydrothermal carbonation

Introduction

Biochar, a carbon-rich material obtained from biomass, is considered a practical carbon reduction method because in addition to its carbon fixation effect, it can apply to many environmental fields, such as soil amendments, remediation of organic and inorganic contaminants, and catalysts (Oliveira et al. 2017; Zhang et al. 2019). Thus, in recent years, the production and utilization of biochar have been getting significant attention due to its environmental aspect and physicochemical properties for engineering applications (Law et al. 2022; Zhang et al. 2019). Biochar can be produced from biomass by thermochemical processes such as dry pyrolysis, gasification, and hydrothermal carbonization (Kumar et al. 2020). The feed biomass and thermochemical conditions would control the yield of biochar as well as its

physicochemical characteristics (Binda et al. 2020; Kumar et al. 2020; Zhang et al. 2019). Depending on the production process and reaction mechanism, biochar can be classified into pyrochar and hydrochar (Kumar et al. 2020). Pyrochar can be produced from dried biomass by dry thermal carbonization (DTC) processes under an oxygen-limited environment at a relatively high temperature of 400–900 °C. On the other hand, hydrochar is produced by a hydrothermal carbonization (HTC) process, in which the reaction is carried out at a relatively low temperature (180–250 °C) and high pressure (2–6 MPa) in the presence of water.

Various types of biomass have been applied for biochar production, such as wood, plants, algae, sewage sludge, and agricultural waste (Guo et al. 2020; Kambo et al. 2015). Among the various feed biomass, microalgal biomass has been considered to be a promising feedstock for biofuel production such as biodiesel, bioethanol, and biochar due to its fast growth rate and high CO₂ fixation efficiency (Bach et al. 2017; Binda et al. 2020; Yu et al. 2017). Microalgal biomass-derived biochar has been known to have less carbon but more nitrogen, ash, and minerals than other lignocellulosic biomass-derived biochar, which could make it suitable for soil amendment and long-term carbon sequestration (Bird et al. 2011; Gan et al. 2018). However, the

Responsible Editor: Zhihong Xu

✉ Eun Jung Kim
ejkim@mokpo.ac.kr

¹ Department of Environmental Engineering, Mokpo National University, 1666 Yongsan-Ro, Cheongye-Myeon, Muan-Gun, Jeollanam-Do 58554, Republic of Korea

high liquid contents (80–90%) of microalgae challenge the thermochemical conversion of microalgal biomass due to the low efficiency and high energy consumption (Bach et al. 2017). Traditional thermochemical processes such as pyrolysis and gasification would not be economically feasible for microalgal biomass with high liquid contents. On the other hand, hydrothermal reactions can be processed without drying, which consumes much energy. Thus, HTC is a promising thermochemical process for producing biochar from wet biomass such as microalgae (Kambo et al. 2015; Khoo et al. 2020; Kumar et al. 2020).

Although microalgal biomass has been getting significant attention as the third-generation feedstock for biofuel production in recent decades, microalgae-derived biochar still needs to be thoroughly understood. Mainly, there is a need for further research on the hydrochar produced from microalgal biomass (Binda et al. 2020; Khoo et al. 2020). Thus, this study aims to evaluate the production and physicochemical properties of microalgae-derived hydrochar by comparison with pyrochar for environmental applications. Various thermochemical process conditions could affect the production and physicochemical properties of biochar. Among them, the temperature is the most critical process condition affecting the properties of the produced biochar because the decomposition, conversion, and removal of volatile substances of biomass components are affected by temperature during biochar production (Bach et al. 2017; Kumar et al. 2020). In this study, hydrochar and pyrochar were produced with commercially available *Chlorella vulgaris* microalgae under various temperature conditions, and their production yield, physicochemical properties, and adsorption characteristics were evaluated for environmental application.

Materials and methods

Biochar production

Hydrochar and pyrochar were produced with commercially available dried microalgal biomass, *Chlorella vulgaris*, provided by Daesang Corporation. The hydrothermal carbonization (HTC) process was conducted using a stainless steel hydrothermal autoclave reactor. Ten grams of biomass and 90 ml of distilled water were mixed into a reactor for 5 min. Then, the reactor was placed in an oven and reacted for 4 h at 140, 170, and 200 °C. The effect of reaction time was evaluated at 170 and 200 °C for 0.5 to 6 h. After the reaction, the mixture was cooled to room temperature, and centrifugation was conducted for solid–liquid separation. The solid particles were washed with distilled water and dried at 105 °C. The dried particles were made into powder using a mortar and pestle and then stored in a desiccator until

characterization. The pH and TOC of the liquid supernatant were analyzed.

The dry thermal carbonization (DTC) process was conducted in a nitrogen environment using a vacuum electric furnace. Five grams of biomass in an aluminum crucible with a lid was placed in an electric furnace, the internal pressure of the furnace was adjusted to –1 bar with a pump, and nitrogen gas was injected. This process was repeated three times to create an anoxic condition inside the electric furnace. Then, the temperature was raised for 30 min to reach the reaction temperatures (300, 400, and 500 °C) and maintained for 1 h. After the reaction, the sample was cooled in an electric furnace to room temperature, washed with acetone and water, and dried at 105 °C. The dried particles were made into powder and stored in a desiccator until characterization.

The following equation calculates the production yield (yield) of pyrochar and hydrochar.

$$\text{Yield (\%)} = \frac{\text{Sample weight after reaction}}{\text{Sample weight before reaction}} \times 100$$

Biochar characterization

Elemental composition, pH, and surface characteristics were analyzed to evaluate the physicochemical properties of the pyrochar and hydrochar. The pH was measured in a 1:10 suspension of biochar in deionized water. The C, H, O, and N elemental compositions of biochar were analyzed using an elemental analyzer (Flash 2000, Thermo Fisher). The surface functional groups of biochar were evaluated using a Fourier transformed infrared (FTIR) spectrometer (Frontier, Perkin Elmer), and the specific surface areas were measured using a BET analyzer (BELSORP-maxII, MicrotracBEL Corp). The surface morphology was studied with a scanning electron microscope (SEM) ((Hitachi S-4800, Japan).

Adsorption experiment

Adsorption experiments for lead (Pb(II)) were conducted to investigate the adsorption characteristics of heavy metals of hydrochar and pyrochar. Lead adsorption kinetics were investigated with 1 g/L of biochar suspensions in 250-mL reaction vessels. Reactions were initiated by adding lead standard solution (Pb(NO₃)₂) to a biochar suspension. The suspension was continuously agitated using a magnetic stirrer throughout the reaction for 24 h. A 10-mL aliquot was sampled from the suspension at each reaction time and immediately filtered using 0.45-μm membrane filters. The effect of initial lead concentrations on lead adsorption by biochar (adsorption isotherm) was studied by varying initial concentrations of

lead. Biochar suspensions (1 g/L) were allowed to react with 20–625 mg/L of lead at pH 5 in 20-mL polyethylene vials, and the suspensions were continuously mixed on a shaker at 150 rpm for 24 h. After the reaction, the suspensions were filtered through 0.45- μm membrane filters. The lead concentrations in the filtrates were measured to determine the extent of lead adsorption using an inductively coupled plasma spectrophotometer (ICP-OES, Agilent 5800).

The adsorption kinetics data were fitted with pseudo-first-order, pseudo-second-order, and intraparticle diffusion models, which were expressed as the following Eqs. 1, 2, and 3, respectively (Ho and McKay 1999; Kołodyńska et al. 2012; Wang and Guo 2022):

$$\ln(q_e - q_t) = \ln q_e - k_1 t \quad (1)$$

$$\frac{t}{q_t} = \frac{1}{k_2 q_e^2} - \frac{t}{q_e} \quad (2)$$

$$q_t = k_i t^{1/2} + C \quad (3)$$

where q_t (mg g^{-1}) is the adsorption amount of lead at time t (min), q_e (mg g^{-1}) is the adsorbed amount of lead at equilibrium, k_1 (min^{-1}) is the pseudo-first-order rate constant, k_2 ($\text{g mg}^{-1} \text{min}^{-1}$) is the pseudo-second-order rate constant, k_i ($\text{mg g}^{-1} \text{min}^{-1/2}$) is the intraparticle diffusion rate constant, and C (mg g^{-1}) is the intercept. The kinetic parameters were calculated by plotting $\log(q_e - q_t)$ vs. t , t/q_t vs. t , and q_t vs. $t^{1/2}$, presented in Table 2.

The adsorption isotherm data were applied to Langmuir (Eq. (4)) and Freundlich (Eq. (5)) to evaluate the adsorption results:

$$q = \frac{q_{\max} b C_e}{1 + b C_e} \quad (4)$$

$$q = K C_e^{1/n} \quad (5)$$

where q is the amount of lead adsorbed per gram of biochar (mg/g), C_e is the concentration of lead in solution at equilibrium (mg/L), q_{\max} is the maximum adsorption amount of lead (mg/g), b is the adsorption constant (L/mg), K is the adsorption capacity, and $1/n$ is the adsorption strength. The values of q_{\max} and b can be determined from the linear plot of C_e/q_e versus C_e , while the values of K_f and n were evaluated from the linear plot of $\ln q_e$ versus $\ln C_e$. The Langmuir model assumes monolayer adsorption at specific homogeneous sites with equal adsorption energy, while the Freundlich model implies multilayer heterogeneous adsorption (Al-Ghouti and Da'ana 2020).

Results and discussions

Production yields

Effects of reaction temperature and reaction time on the production yields of hydrochar and pyrochar from microalgae were evaluated under various reaction temperatures and reaction times. Figure 1 shows the % yields of hydrochar and TOC levels of the process water produced from microalgae by the HTC process under various reaction temperatures (140, 170, and 200 °C) and reaction times (up to 6 h). The hydrochar yields decreased as the reaction temperature and time increased, similar to the previous studies (Fig. 1a, c) (Bach et al. 2017; de Siqueira Castro et al. 2021; Liu et al. 2019). At the same time, TOC levels of the aqueous phases increased at higher temperatures and longer reaction times, opposite to the production yields (Fig. 1b, d). The production yields were decreased from 61 to 32% as the reaction temperature was increased from 140 to 200 °C, while TOC levels were increased from 16 to 25 g/L as the temperature was increased. At 200 °C, the hydrochar production yield rapidly decreased as the reaction continued for 2 h, but after 2 h, the yield remained almost constant. At the same time, TOC levels of the aqueous phase showed a rapid increase as the reaction continued for 2 h, and later, only a slight rise in the TOC levels was observed. On the other hand, at 170 °C, the yields were continuously decreased for 4 h. Similarly, an increase in TOC concentrations in the aqueous phase was observed for 4 h.

The decrease in production yield (decrease in biomass weight after the reaction) during the HTC process is mainly caused by the decomposition of biomass via dehydration or decarboxylation reactions (Liu et al. 2019). The higher yield was observed at low temperatures and the early reaction, possibly due to the partial decomposition of the biomass polymer at the early stage of reaction and low temperature. However, more dehydration or decarboxylation reactions could occur as the reaction continues at high temperatures, which resulted in lower production yield. The resulting organic and inorganic matter from biomass degradation could be dissolved in the aqueous phase, as indicated in high TOC levels at high temperatures (Sevilla and Fuertes 2009). In addition, a decrease in the pH of the process water is known to be due to the formation of organic acids such as acetic, formic, and lactic acids during biomass degradation (Jain et al. 2016).

Figure 2 shows the % yield of pyrochar produced from microalgae by DTC for 1 h under various temperatures from 300 to 500 °C and the % yield at different reaction times up to 3 h at 400 °C. Pyrochar yields decreased from 55 to 29% with pyrolysis temperature increased from 300

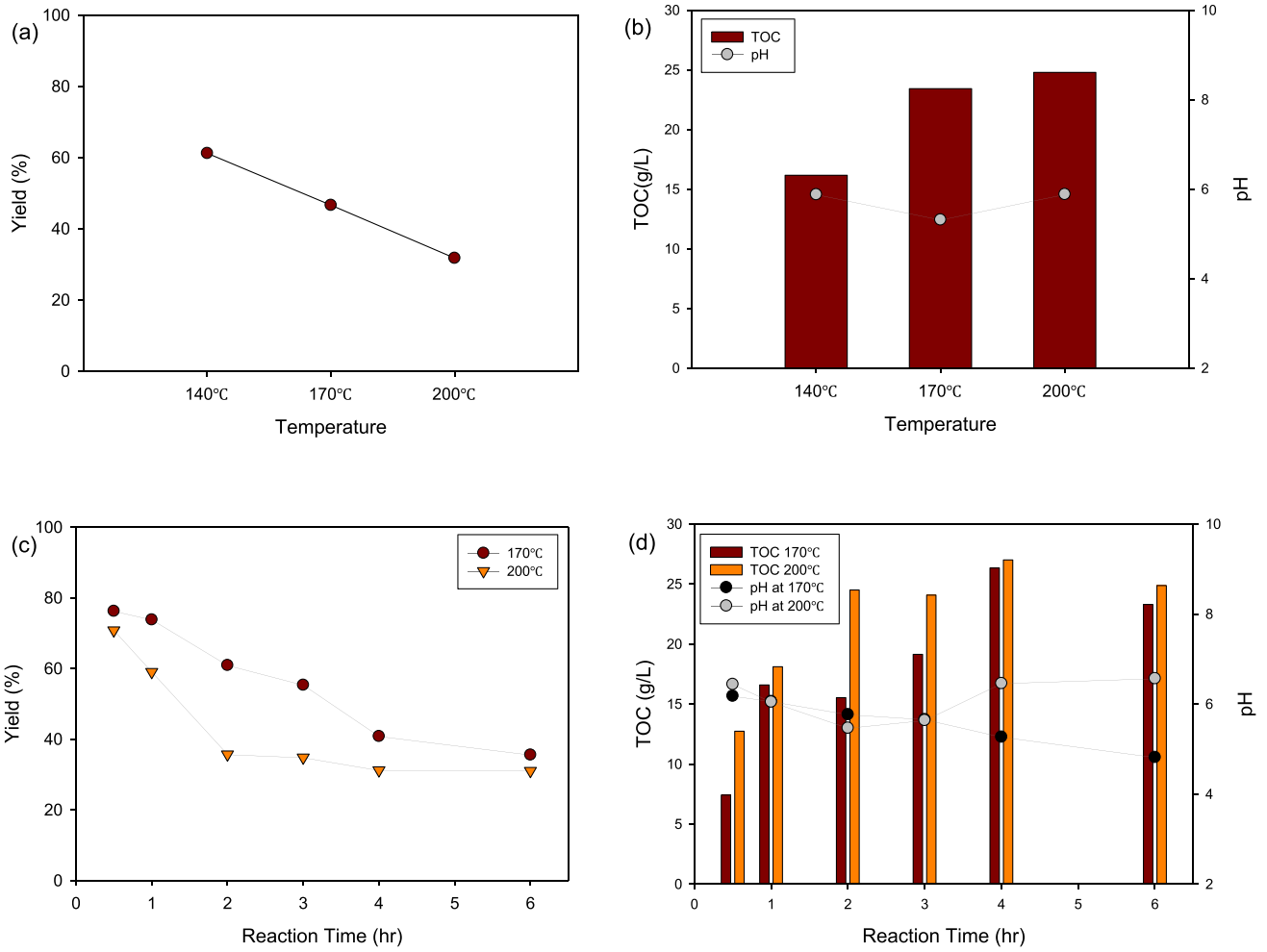


Fig. 1 Effects of temperature and reaction time on **a, c** yields of hydrochar and **b, d** TOC concentrations of process water produced from microalgae

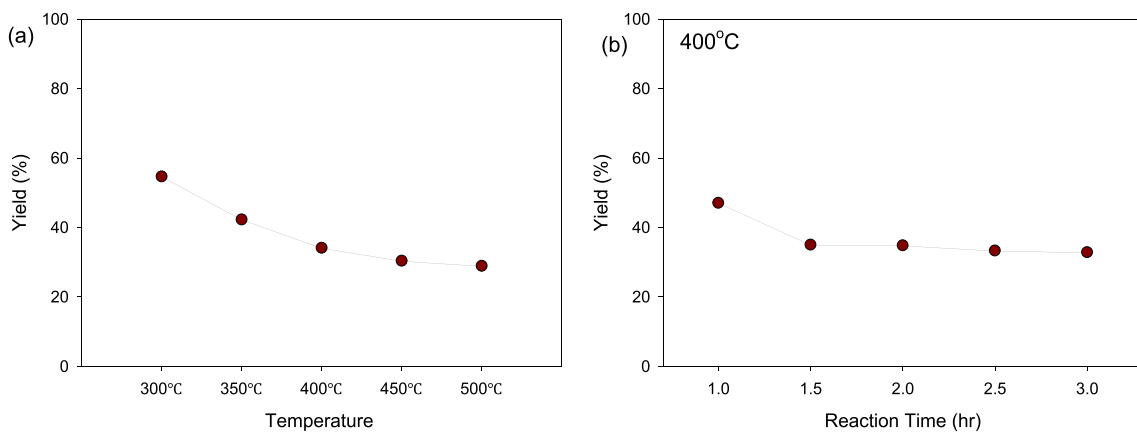


Fig. 2 Effect of **a** temperature and **b** reaction time on yields of pyrochar produced from microalgae

to 500 °C, which were lower than those of hydrochar in this study but similar to that of *C. vulgaris* pyrolyzed at 350 °C in a previous study (Binda et al. 2020). When the reaction was conducted for 1 to 4 h at 400 °C, the yield reduced from 47 to 35% as the reaction continued from 1 to 1.5 h, but later, the yield remained almost constant. The reduction of the production yield is due to the loss of volatile matter and the decomposition of biomass (Kwak et al. 2019). The results indicated that biomass was fully carbonized in 1.5 h at 400 °C. Overall, HTC showed a higher yield than DTC, which is believed to be due to carbonization at a low temperature.

Physicochemical properties of biochar

The physicochemical characteristics of biochar are essential for its application, which includes surface area, porosity, pH, elemental composition, functional groups, and ash contents (Guo et al. 2020; Li et al. 2017). The biochar production mechanism by HTC and DTC processes and reaction conditions could affect the physicochemical properties of biochar (Kumar et al. 2020).

Table 1 shows the physicochemical properties of microalgal hydrochar and pyrochar produced under various thermochemical conditions. Ash contents of hydrochar decreased from 12.1 to 7.35% as reaction temperature increased from 140 to 200 °C. On the other hand, ash contents of pyrochar rose from 15.2 to 19.0% as the reaction temperature increased from 300 to 500 °C. Hydrochar showed lower ash contents than raw biomass or pyrochar, which might be due to the dissolution of small inorganic and/or organic compounds produced from the decomposition of biomass during the HTC process in the aqueous phase (Belete et al. 2019). More decomposition of biomass at higher temperatures could produce more soluble inorganic compounds, which seemed to result in lower ash contents of the hydrochar at higher temperatures. On the other hand, higher ash contents of pyrochar at higher reaction temperatures could be due to the fast decomposition of biomass under higher

temperatures, which resulted in lower organic matter and higher ash contents (Kwak et al. 2019; Liu et al. 2019).

Carbon contents increased after carbonization by both DTC and HTC processes compared to the raw biomass and increased as reaction temperature increased. Carbon contents of hydrochar rose from 52.8 to 65.6% as the reaction temperature increased from 140 to 200 °C, while those of pyrochar rose from 66.6 to 67.3% as the reaction temperature increased from 300 to 500 °C. Hydrogen contents of hydrochar increased as reaction temperature increased, while those of pyrochar decreased. The oxygen contents of both hydrochar and pyrochar decreased with increasing temperature. The hydrogen and oxygen contents of hydrochar were similar to those of raw biomass except for lower oxygen in hydrochar produced at 200 °C. At the same time, those of pyrochar were significantly reduced compared to those of raw biomass. During thermal carbonization processes, variations of elemental contents mainly occur through dehydration and decarboxylation reactions (de Siqueira Castro et al. 2021). The increase in carbon contents could be due to condensation and aromatization, while the decrease in oxygen and hydrogen contents could be caused by dehydration and decarboxylation (Binda et al. 2020; Liu et al. 2019). In other words, the decrease in oxygen to carbon ratio (O/C) value indicates dehydration and decarboxylation, and the reduction in hydrogen to carbon ratio (H/C) value is related to dehydration and a degree of aromatization (Liu et al. 2019). The values of O/C and H/C of hydrochar were 0.179–0.350 and 0.133–0.152, respectively, which were higher than those of pyrochar having O/C and H/C values of 0.002–0.008 and 0.039–0.091, respectively. HTC and DTC processes resulted in lower O/C and H/C values than raw biomass, but hydrochar resulted in higher O/C and H/C than pyrochar. This result indicates that hydrochar has more hydrophilic surface properties than pyrochar, favoring the adsorption of heavy metals. The low O/C and H/C fractions of pyrochar indicate that intensive dehydration and decarboxylation occurred during the DTC process, which would contribute to the higher aromaticity and lower polarity of the pyrochar. It was

Table 1 Physicochemical properties of hydrochar and pyrochar produced at various temperature conditions from microalgae

Parameters	Unit	Biomass	Hydrochar			Pyrochar		
			140 °C	170 °C	200 °C	300 °C	400 °C	500 °C
Ash	%	12.3	12.1	10.5	7.35	15.2	17.0	19.0
C	%	49.1	52.8	57.0	65.6	66.6	67.4	67.3
H	%	7.64	8.01	8.30	8.75	6.03	4.11	2.62
O	%	21.1	18.5	16.2	11.7	0.52	0.18	0.16
N	%	9.85	8.56	8.08	6.60	11.65	11.35	10.94
O/C		0.431	0.350	0.284	0.179	0.008	0.003	0.002
H/C		0.156	0.152	0.146	0.133	0.091	0.061	0.039
pH		6.17	5.23	4.54	4.46	6.40	5.84	5.87
Surface area	m ² /g	0.221	0.0576	0.151	0.191	0.280	0.405	0.313

also observed that an increase in the temperature of HTC and DTC resulted in a decrease in the O/C and H/C values, which suggests an increase in the degree of condensation of the hydrochar and pyrochar at high temperatures (Sevilla and Fuertes 2009).

The pH values of the biochar produced in this study were 4.46 to 6.40, which is neutral to slightly acidic. The pH of the biochar has been reported to be affected by the types of feedstock and pyrolysis temperature (Kwak et al. 2019; Li et al. 2017). The pH of the hydrochar was 3.85–4.84, which was lower than that of pyrochar (pH 5.84–6.40). The pH of biochar has been known to have a positive correlation with the ash content (Li et al. 2017). The ash contents of hydrochar (7.35–12.1%) were lower than those of pyrochar (15.2–19.0%), which could influence the lower pH of hydrochar than pyrochar. In addition, a decrease in acidic functional groups on the surface due to polymerization and dehydration during the carbonization process could affect the pH of biochar (Li et al. 2017). The presence of acidic functional groups on the surface of hydrochar seemed to contribute to the low pH of hydrochar (shown in the FTIR in “FTIR investigation of biochar”).

The specific surface areas of hydrochar were 0.058–0.191 m²/g, which were lower than those of raw biomass (0.22 m²/g). Although pyrochar presented higher surface areas with 0.28–0.405 m²/g than raw biomass or hydrochar, its surface area was relatively low compared to those of other algal biochar (1.15–4.26 m²/g) or other biomass-derived

biochar (0.9–491 m²/g) (Ahmad et al. 2014; Bird et al. 2011). The specific surface area of biochar is affected by carbonization temperature and feed biomass composition (Ahmad et al. 2014). The surface area generally increases with increased reaction temperature because more pores are created at higher temperatures. In this study, hydrochar and pyrochar surface areas slightly increased at higher reaction temperatures, but the low surface areas seemed to be mainly affected by algal feed biomass. In addition, the lower specific surface area of hydrochar than pyrochar could be due to the poor development of pores during the HTC process (Hung et al. 2017; Kambo et al. 2015).

SEM was used to study the morphology of solid products (Fig. 3). Raw biomass presented a spherical shape with a relatively smooth surface with furrows. Hydrochar produced at 170 °C consisted mainly of aggregates of microspheres with rugose characters with a 2–3- μ m diameter. Hydrochar at 200 °C exhibited clusters of irregular shapes presenting high rugulose on the surface. During the HTC process, the roughness of the surface increased consistent with the increase of specific surface area as reaction temperature increased, which could be potential reactive sites at higher reaction temperatures. On the other hand, pyrochar presented irregular shapes and sizes with some pores and graphite-like sheet structures similar to the previous study (Binda et al. 2020). These observations confirmed the influence of carbonization methods and carbonization temperature on the morphology of biochar.

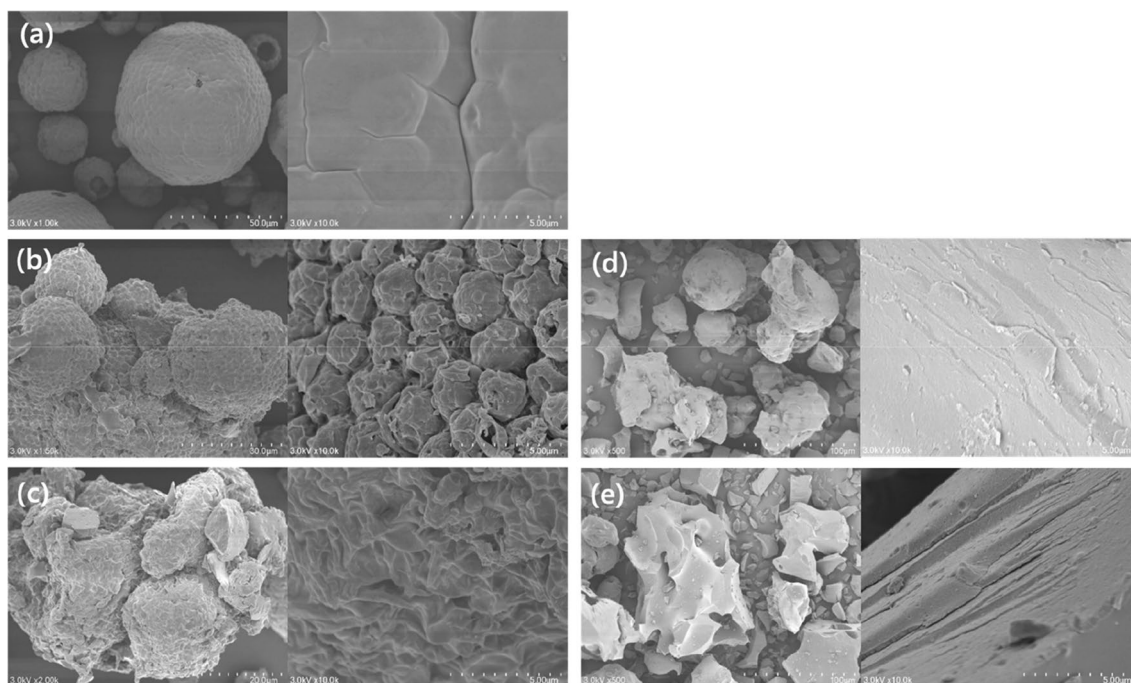


Fig. 3 SEM images of **a** raw biomass, **b** hydrochar produced at 170 °C for 4 h, **c** hydrochar produced at 200 °C for 4 h, **d** pyrochar produced at 300 °C for 1 h, and **e** pyrochar produced at 400 °C for 1 h

FTIR investigation of biochar

Functional groups on the surface of biochar are essential in determining hydrophobic or hydrophilic properties of the surface as well as their interaction with contaminants such as heavy metals. Figure 4 shows FTIR spectra of raw microalgal biomass and biochar (hydrochar and pyrochar) produced from microalgae at various temperatures. The FTIR spectrum of raw biomass mainly presented the following: (i) broadband regions of $3600\text{--}3000\text{ cm}^{-1}$, associated with --OH bonds in hydroxyl and carboxylic acid bands; (ii) aliphatic C--H stretching bands at 2922 and 2852 cm^{-1} related methyl and methylene groups of fatty acids; (iii) C=C , C=O , and N--H functional groups of aromatic and amide at 1640 , 1543 , 1440 cm^{-1} ; (iv) C--O--C stretching band present in cellulose at the position of 1020 cm^{-1} (Binda et al. 2020; Keiluweit et al. 2010; Khoo et al. 2020). These functional groups analyzed by FTIR can be divided into biochemical components of lipid ($3600\text{--}2850\text{ cm}^{-1}$), protein ($1640\text{--}1410\text{ cm}^{-1}$), and carbohydrate ($1113\text{--}1007\text{ cm}^{-1}$) (Khoo et al. 2020).

The FTIR spectra of hydrochar showed that the intensities of the peaks in the regions of lipid ($3600\text{--}2850\text{ cm}^{-1}$) and protein ($1640\text{--}1410\text{ cm}^{-1}$) increased with the increase of reaction temperature from 140 to $200\text{ }^{\circ}\text{C}$, while the peaks in the carbohydrate ($1113\text{--}1007\text{ cm}^{-1}$) region decreased with the temperature rise (Fig. 4a). This is also observed with the increase of reaction time from 0.5 to 6 h at $170\text{ }^{\circ}\text{C}$ (Fig. 5). As the reaction time increases, the intensities of peaks in the carbohydrate region weaken, while those in the protein

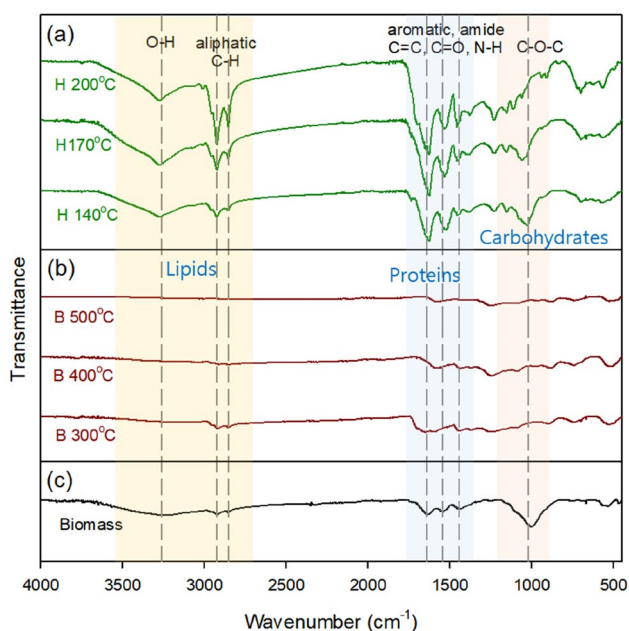


Fig. 4 FTIR spectra of **a** hydrochar and **b** pyrochar produced at various temperatures, and **c** raw algal biomass

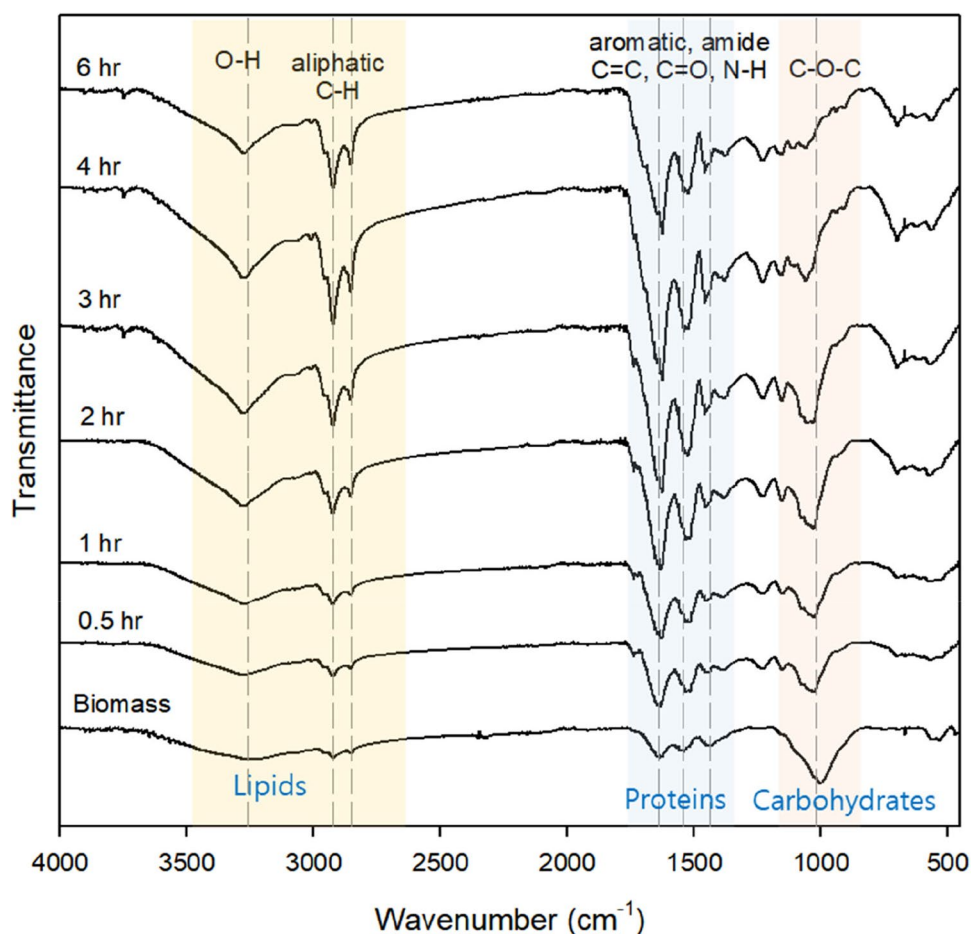
and lipid regions get stronger. The increase of aliphatic C--H (2922 and 2852 cm^{-1}) intensity indicates that the hydrolysis of the polymer occurred by the HTC process, and the enhancement of aromatic C=C region ($1640\text{--}1410\text{ cm}^{-1}$) shows the increase of hydrophobicity and development of aromatization of hydrochar at the high-temperature reaction (Liu et al. 2019). Therefore, aliphatic C--H and aromatic C=C enhancement at high temperatures indicate condensation and aromatization. At the same time, the decrease of the C--O--C stretching band (1020 cm^{-1}) at high temperatures indicates the decomposition of C--O--C in carbohydrates during the hydrothermal reaction. In addition, compared to the raw biomass, hydrochar showed several peaks at $1100\text{--}1300\text{ cm}^{-1}$ regions, possibly related to aromatic C--H stretching, and their intensities increase as the reaction temperature increases.

On the other hand, the FTIR spectra of pyrochar showed a decrease in intensities of all the lipid, protein, and carbohydrate regions with increased temperature. At $500\text{ }^{\circ}\text{C}$, only peaks at the aromatic C=C region were observed, indicating intensive dehydration and decarboxylation reactions and an increase of hydrophobicity and aromatization during the DTC process. These results are consistent with the elemental compositions showing that carbon was mainly present for the pyrochar produced at $500\text{ }^{\circ}\text{C}$ (Table 1). Overall, the FTIR results demonstrate the qualitative differences in the surface functional groups between hydrochar and pyrochar, possibly due to the differences in the carbonization conditions. Compared to the pyrochar, the surface of hydrochar presented more oxygen-containing functional groups in the region of lipid and protein (--OH , C=O , and N--H functional groups), which would be beneficial for water affinity and metal adsorption (Zhang et al. 2019).

Adsorption characteristics of biochar

Adsorption experiments for lead (Pb(II)) were conducted to investigate the adsorption characteristics of heavy metals of hydrochar and pyrochar. Lead was chosen as the subject of study to investigate the adsorption properties of biochar. This is because lead contamination in water and soil has become a significant concern in many parts of the world, and biochar has been proposed as a potential adsorbent for the removal of lead (Kwak et al. 2019; Lu et al. 2012). The physicochemical properties of biochar significantly determine their adsorption capacity, efficiency, and adsorptive mechanisms (Law et al. 2022). Time-dependent lead adsorption was studied with hydrochar produced at $200\text{ }^{\circ}\text{C}$ and pyrochar made at $400\text{ }^{\circ}\text{C}$ for 24 h (Fig. 6a). Adsorption of lead by hydrochar was fast initially, with over 90% of the highest adsorption occurring in the first 60 min , followed by very slow adsorption during the rest of the reaction time. The initial rapid adsorption suggested that the adsorption

Fig. 5 FTIR spectra of hydrochar reacted for various reaction times at 170 °C



happened at the surface rather than in the micropores, which is consistent with the observation of poor development of pores for the hydrochar. On the other hand, pyrochar showed the initial adsorption of lead with about 40% of the ultimate lead adsorption within 30 min and continued slow adsorption for the rest of the reaction time.

Adsorption of lead in the solution by biochar can occur as the following three processes: (i) the transport of lead in the solution to the external surface of the biochar (film diffusion); (ii) the transport of lead into the pores of the biochar (intraparticle diffusion); (iii) the adsorption of lead on the active sites of the biochar (Kołodyńska et al. 2012; Wang and Guo 2022). To understand the lead adsorption process by biochar, the adsorption kinetics data were fitted with pseudo-first-order, pseudo-second-order, and intraparticle diffusion models, and the kinetic parameters are presented in Table 2. Among the kinetic models, the adsorption of lead by hydrochar was described best by a pseudo-second-order model with the highest correlation coefficient (R^2) values and good agreement between estimated q_e and experimental q_e . This suggests that the rate-limit stage of lead adsorption on hydrochar was the adsorption on the active sites of the hydrochar surface (chemisorption), which involves surface complexation

reactions at specific sorption sites (Kwak et al. 2019). On the other hand, the intraparticle diffusion model better-described lead adsorption by pyrochar, which indicates that the internal diffusion process mainly controlled the adsorption rate. The different pyrolysis conditions between hydrochar and pyrochar resulted in different pore structures and surface characteristics, which could affect the adsorption mechanisms and rates. The large presence of oxygen-containing functional groups on the surface of hydrochar, as discussed in the FTIR investigation, seemed to play an important role in lead adsorption by complexation. In contrast, lead adsorption by pyrochar seemed to be controlled by intraparticle diffusion due to the fewer functional groups on the surface and more development of the pore structure of pyrochar.

The effect of initial lead concentrations on lead adsorption by biochar was studied at different initial lead concentrations ranging from 0 to 625 mg/L (Fig. 6b). The amounts of lead adsorbed (q) to hydrochar and pyrochar were increased as the initial lead concentrations increased. Table 3 shows the results obtained when the Langmuir and Freundlich isotherm adsorption models were applied to the adsorption results. Correlation coefficients (R^2) suggested that the Langmuir model better fitted the lead adsorption

Fig. 6 Lead adsorption on hydrochar synthesized at 200 °C and pyrochar synthesized at 400 °C. **a** Effect of reaction time, **b** effect of initial concentration of lead

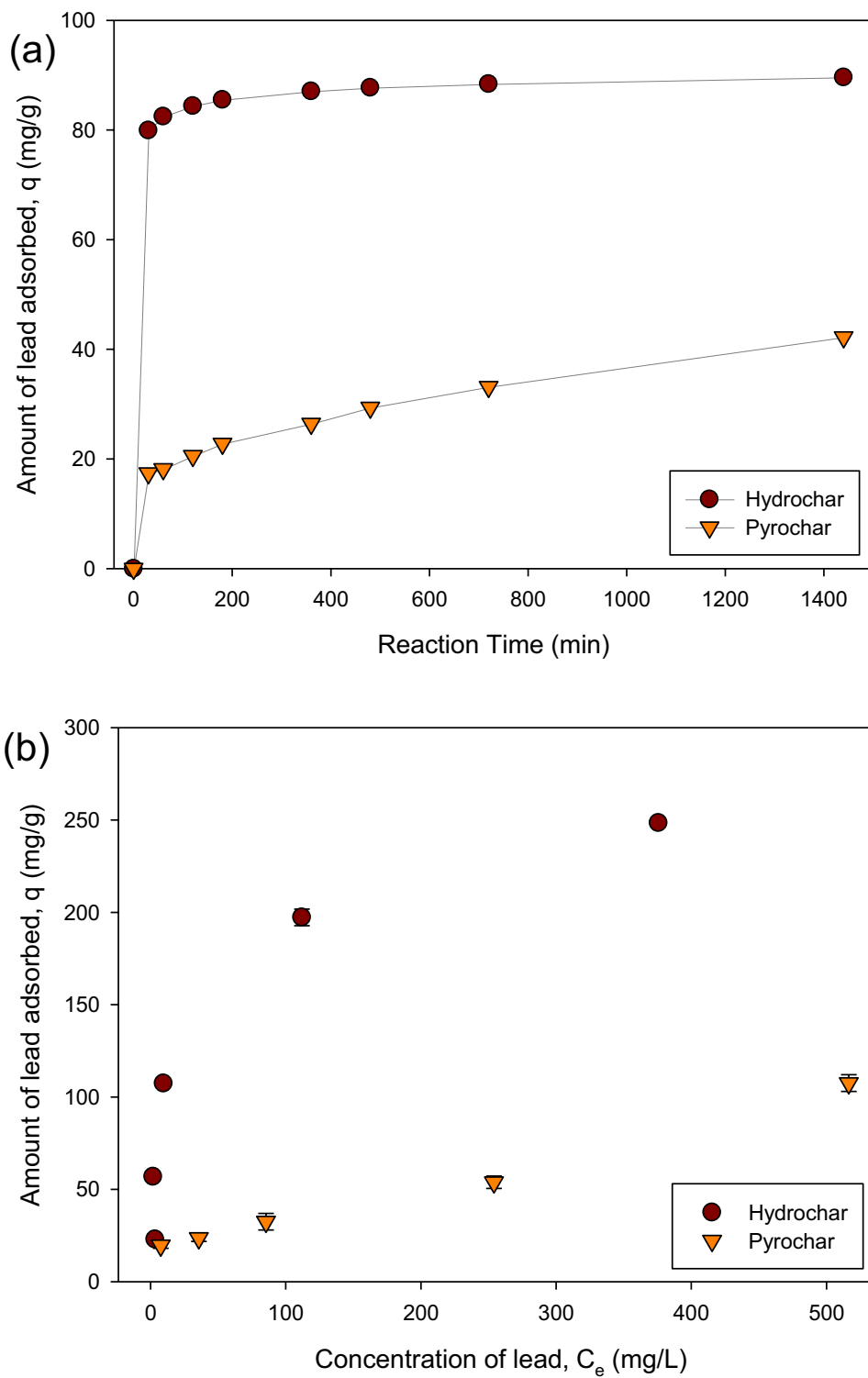
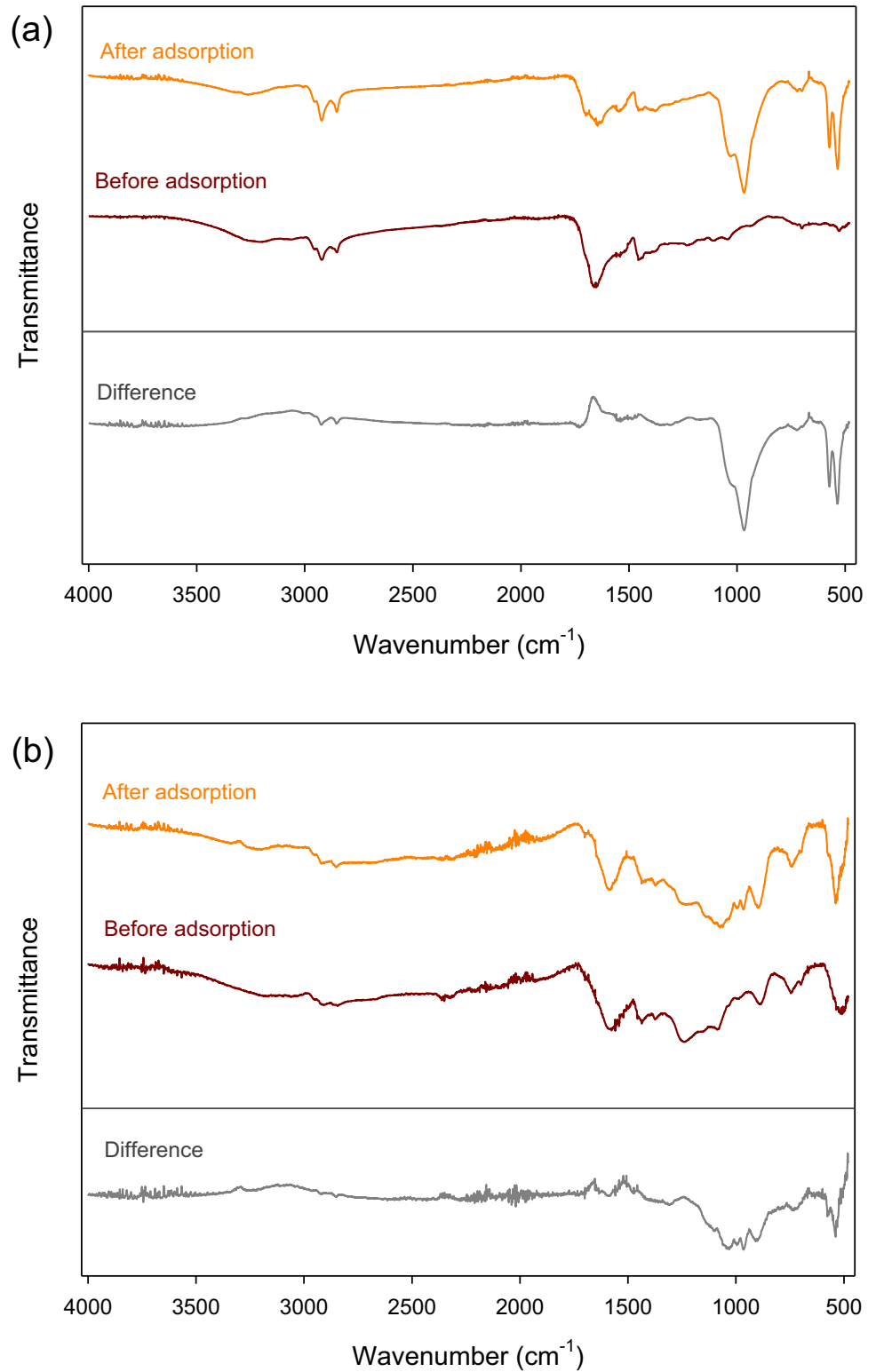


Table 2 Parameters of adsorption kinetic models

	Pseudo-first-order			Pseudo-second-order			Intraparticle diffusion		
	q_e	k_1	R^2	q_e	k_2	R^2	k_i	C	R^2
Hydrochar	11.74	0.0050	0.9522	90.09	0.0013	0.9999	0.2717	80.88	0.8281
Pyrochar	30.81	0.0022	0.9632	44.05	0.0002	0.9711	0.7778	12.33	0.9974

Table 3 Parameters of adsorption isotherm models

	Langmuir			Freundlich		
	q_{max}	b	R^2	K	n	R^2
Hydrochar	263.2	0.0461	0.9937	31.30	2.709	0.7639
Pyrochar	123.5	0.0060	0.7590	7.176	2.588	0.8768

Fig. 7 FTIR spectra before and after lead (Pb(II)) adsorption on **a** hydrochar synthesized at 200 °C and **b** pyrochar synthesized at 400 °C

on hydrochar, while the Freundlich model better fitted the lead adsorption on pyrochar. These isotherm model results indicate that lead adsorption by hydrochar seemed to be achieved by binding to the adsorption sites, such as surface functional groups present on the surface of the hydrochar in a monolayer. On the other hand, lead removal by pyrochar seemed to occur mainly by a multilayer heterogeneous adsorption process.

The highest lead adsorption amounts (q) were 248.4 mg/g for hydrochar and 107.5 mg/g for pyrochar, indicating that the adsorption of lead by hydrochar was more effective than pyrochar. In addition, compared to the lead adsorptions by other biochars prepared from various biomass (2.3–140 mg/g) (Kwak et al. 2019; Lu et al. 2012), it is clear that the microalgal hydrochar produced in the current study is effective for lead adsorption. In the adsorption of biochar, functional groups and surface area are known to be the essential characteristics of biochar (Kwak et al. 2019; Li et al. 2017). Even though pyrochar presented a larger surface area (0.405 m²/g) than hydrochar (0.191 m²/g), higher lead adsorption of hydrochar than pyrochar could be due to the presence of more oxygen-containing functional groups in the surface of hydrochar, which could play beneficial affect role in lead adsorption.

FTIR spectra obtained for hydrochar and pyrochar were compared before and after lead adsorption (Fig. 7). After lead adsorption, the FTIR spectra of hydrochar and pyrochar showed a significant increase of the transmittance intensities in the band regions of 750–1100 and 450–600 cm⁻¹, while a decrease of the transmittance intensity in the band region of 1640–1410 cm⁻¹. The 1640–1410 cm⁻¹ region is associated with C=C, C=O, and N–H functional groups of aromatic and amide. The decrease in this region indicated that those functional groups could participate in lead adsorption. The wavenumber region between 750 and 1100 cm⁻¹ is related to the C–OPb stretching band, while the region 450–600 cm⁻¹ is reported to be associated metal–O band, probably Pb–O in this study (Senvaitiene et al. 2007; Shi et al. 2018). The increase of the C–OPb stretching band intensities after lead adsorption indicates that lead can be removed by hydrochar and pyrochar by complexation reaction with surface functional groups like C=O and present on the surface as C–OPb. Also, the increase of the Pb–O band indicates that lead was removed by precipitation reaction and present as the PbO phase on the biochar surface.

Conclusions

In this study, microalgal biochar was produced with commercially available microalga, *C. vulgaris*, using HTC and DTC processes under various temperature conditions, and

production yields, physicochemical properties, and hydrochar and pyrochar adsorption characteristics were evaluated. The HTC process resulted in a higher production yield than the DTC process, possibly due to the low-temperature carbonization. Pyrochar presented higher pH, ash contents, porosity, and surface area than hydrochar. Hydrochar presented more oxygen-containing functional groups on the surface than pyrochar, which could play a beneficial role in lead adsorption by hydrochar. Hydrochar produced from microalgae in the current study was quite effective for lead adsorption compared to the microalgal pyrochar in this study and other biochar in previous studies. Thus, our results suggest that HTC could be an economically feasible thermochemical process for microalgal biochar production. It can produce hydrochar with high production yield from wet microalgae at low temperatures without a drying process. The hydrochar produced from microalgae could be effectively applied in soil amendment and various environmental remediations.

Author contribution All authors contributed to the study conception and design. Material preparation, data collection, and analysis were performed by Chaerin Park and Eun Jung Kim. The first draft of the manuscript was written by Chaerin Park, and all authors commented on previous versions of the manuscript. All authors read and approved the final manuscript.

Funding This work was supported by the Korea Environment Industry & Technology Institute (KEITI) through Project to develop eco-friendly new materials and processing technology derived from wildlife, funded by the Korea Ministry of Environment (MOE) (2021003280005) and partly by the National Research Foundation of Korea (NRF) grants (2019R1F1A1062675).

Declarations

Ethical approval and consent to participate This manuscript has not been published or presented elsewhere in part or entirety and is not under consideration by another journal. All study participants provided informed consent, and the study design was approved by the appropriate ethics review board.

Consent for publication We have read and understood your journal's policies, and we believe that neither the manuscript nor the study violates any of these.

Competing interests The authors declare no competing interests.

References

- Ahmad M et al (2014) Biochar as a sorbent for contaminant management in soil and water: a review. *Chemosphere* 99:19–33
- Al-Ghouti MA, Da'ana D (2020) Guidelines for the use and interpretation of adsorption isotherm models: a review. *J Hazard Mater* 393:122383
- Bach Q-V et al (2017) Wet torrefaction of microalga *Chlorella vulgaris* ESP-31 with microwave-assisted heating. *Energy Convers Manag* 141:163–170

- Belete YZ et al (2019) Characterization and utilization of hydrothermal carbonization aqueous phase as nutrient source for microalgal growth. *Biores Technol* 290:121758
- Binda G et al (2020) Comprehensive comparison of microalgae-derived biochar from different feedstocks: a prospective study for future environmental applications. *Algal Res* 52:102103
- Bird MI et al (2011) Algal biochar—production and properties. *Biores Technol* 102:1886–1891
- de Siqueira CJ et al (2021) Hydrothermal carbonization of microalgae biomass produced in agro-industrial effluent: products, characterization and applications. *Sci Total Environ* 768:144480
- Gan YY et al (2018) Torrefaction of microalgal biochar as potential coal fuel and application as bio-adsorbent. *Energy Convers Manag* 165:152–162
- Guo X-x et al (2020) The role of biochar in organic waste composting and soil improvement: a review. *Waste Manag* 102:884–899
- Ho Y-S, McKay G (1999) Pseudo-second order model for sorption processes. *Process Bioch* 34:451–465
- Hung C-Y et al (2017) Characterization of biochar prepared from biogas digestate. *Waste Manag* 66:53–60
- Jain A et al (2016) Hydrothermal conversion of biomass waste to activated carbon with high porosity: a review. *Chem Eng J* 283:789–805
- Kambo HS et al (2015) A comparative review of biochar and hydrochar in terms of production, physico-chemical properties and applications 45:359–378
- Keiluweit M et al (2010) Dynamic molecular structure of plant biomass-derived black carbon (biochar). *Environ Sci Technol* 44:1247–1253
- Khoo CG et al (2020) Hydrochar production from high-ash low-lipid microalgal biomass via hydrothermal carbonization: effects of operational parameters and products characterization. *Environ Res* 188:109828
- Kołodziejńska D et al (2012) Kinetic and adsorptive characterization of biochar in metal ions removal. *Chem Eng J* 197:295–305
- Kumar A et al (2020) Hydrochar and biochar: production, physicochemical properties and techno-economic analysis. *Biores Technol* 310:123442
- Kwak J-H et al (2019) Biochar properties and lead (II) adsorption capacity depend on feedstock type, pyrolysis temperature, and steam activation. *Chemosphere* 231:393–404
- Law XN et al (2022) Microalgal-based biochar in wastewater remediation: Its synthesis, characterization and applications. *Environ Res* 204:111966
- Li H et al (2017) Mechanisms of metal sorption by biochars: biochar characteristics and modifications. *Chemosphere* 178:466–478
- Liu H et al (2019) Hydrothermal carbonization of natural microalgae containing a high ash content. *Fuel* 249:441–448
- Lu H et al (2012) Relative distribution of Pb²⁺ sorption mechanisms by sludge-derived biochar. *Water Res* 46:854–862
- Oliveira FR et al (2017) Environmental application of biochar: current status and perspectives. *Biores Technol* 246:110–122
- Senvaitiene J et al (2007) XRD and FTIR characterisation of lead oxide-based pigments and glazes. *Acta Chimica Slovenica* 54
- Sevilla M, Fuertes ABC (2009) The production of carbon materials by hydrothermal carbonization of cellulose. *Carbon* 47:2281–2289
- Shi Q et al (2018) Mechanistic study of lead adsorption on activated carbon. *Langmuir* 34:13565–13573
- Wang J, Guo XJC (2022) Rethinking of the intraparticle diffusion adsorption kinetics model: Interpretation, solving methods and applications. *Chemosphere* 309:136732
- Yu KL et al (2017) Recent developments on algal biochar production and characterization. *Biores Technol* 246:2–11
- Zhang Z et al (2019) Insights into biochar and hydrochar production and applications: A review. *Energy* 171:581–598

Publisher's Note Springer Nature remains neutral with regard to jurisdictional claims in published maps and institutional affiliations.

Springer Nature or its licensor (e.g. a society or other partner) holds exclusive rights to this article under a publishing agreement with the author(s) or other rightsholder(s); author self-archiving of the accepted manuscript version of this article is solely governed by the terms of such publishing agreement and applicable law.